namics have not been removed by the dehydroxylation treatments. Peri[3] found that temperatures of 400 °C would successfully remove all physisorbed water, but not all surface hydroxyl groups, and that aluminas dried above 650 °C would still contain isolated hydroxyl groups. At temperatures above 1000 °C, hydroxyl groups continue to combine and traces of water can still be removed from the alumina surface. Given this, the PDA sample will contain a small population of surface hydroxyls as isolated and perhaps neighboring hydroxyl groups, while the IDA and EDA samples may only have isolated hydroxyl groups present. In the case of the dehydroxylated samples, the second type of dynamics, i.e., proton hopping (Schemes 2 and 3), can be envisioned to occur at a faster rate than on the fully hydroxylated samples which have physisorbed water on the surface. This is because there are more neighboring defect sites into which the protons can move.

It has been suggested that there are different types of defect or strain sites on the surface which are responsible for catalytic activity.[7] The surface strain caused by some sites is larger than from other sites, and it is likely that protons would preferentially move to the more strained sites in order to minimize the strain, and thus the total energy of the system. The protons on the untreated surfaces would have only those defect sites which were produced by the initial heating process used to make the catalytic surfaces in which to move. These surface protons are also in competition with the physisorbed water. The protons remaining on dehydroxylated surfaces would not have their motion as inhibited or constrained but would be able to move about the surface more freely as the hydroxyl population decreases and the number of vacant surface defect sites increases. The population of Lewis acid sites on dehydroxylated surfaces is at least as large as untreated surfaces. As we have seen from MO calculations these types of sites give rise to the largest Q_{cc}'s, thereby broadening the signal more than for the untreated surfaces. Thus, we see an even further decrease in the signal intensity of the dehydroxylated samples vs α-alumina at room temperature than with the untreated γ-alumina due to the increased effect of the surface dynamics as well as the increase in the Lewis acid site population. Dehydroxylation increasing in concert with signal intensity may indicate that since the overall surface hydroxyl population is lowered, the average aluminum atom at the surface does not "feel" the effects of the proton motion as much. Also, the surface area of the dehydroxylated samples decreases from PDA to EDA, giving rise to the same effect as is seen for the untreated transition-aluminas as one goes to lower surface area.

Summary and Conclusions

The history of alumina use in catalytic systems is long-lived. However, the understanding of the reaction mechanisms involved in these systems is still in its infancy. Through the use of variable-temperature solid-state ^{27}Al NMR, we have shown that the surface of transition-aluminas may be described as being dynamic. This study was concerned with lateral surface proton motion, where it was assumed that any interstitial migration of protons would occur at a much slower rate and would not have a significant effect on the ^{27}Al NMR signal. The nature of the lateral surface dynamics is manifested in the mobility of surface protons, which are derived from either physisorbed or chemisorbed water. This motion produces an efficient quadrupolar relaxation pathway and aids in the exchange of one type of surface aluminum with another, which results in a broadened line shape and loss in signal intensity. Because these are surface effects, the ^{27}Al NMR signal intensity decreases with increasing surface area. Lowering the temperature to 90 K significantly reduces surface proton mobility, which is shown as a greater than calculated increase in signal for aluminas other than α-alumina. Such dynamics must, therefore, be accounted for in any formulation of a model of the surface of an alumina.

Acknowledgment. We gratefully acknowledge support from the National Science Foundation via Grants CHE85-44272, CHE86-11306, and CHE89-21632. Further, we acknowledge the efforts of John C. Edwards during the initial stages of this research. We also give Dr. Murray Smigel of Convex Computer Corp. special acknowledgment for his help with the MO calculations described and the generous donation of the needed computer time.

Registry No. Al_2O_3, 1344-28-1.

Selective Shaped Pulse Decoupling in NMR: Homonuclear [^{13}C]Carbonyl Decoupling

M. A. McCoy* and L. Mueller

Contribution from Bristol-Myers Squibb Pharmaceutical Research Institute, P.O. Box 4000, Princeton, New Jersey 08543. *Received June 20, 1991*

Abstract: We introduce a novel pulse sequence that is capable of frequency-selective spin decoupling. This sequence uses radio-frequency pulse shaping to greatly attenuate off-resonance side bands which are inherent in broad-band decoupling sequences but, within the bandwidth of the sequence, retains the quality of decoupling possible with the commonly used WALTZ-16 sequence. Selective carbonyl decoupling is demonstrated in a heteronuclear multiple quantum correlation experiment where it is shown that efficient decoupling of the carbonyl from the Cα carbons occurs without distorting nearby aromatic coherences. Selective decoupling promises to be a powerful new tool in high-resolution spectroscopy and especially in protein NMR where it is possible to remove the effects of undesirable isotopic labels.

In NMR experiments on ^{13}C- and ^{15}N-labeled proteins, the large homonuclear carbonyl coupling to the C_α carbon ($J_{CC} \sim 60$ Hz) and, to a lesser extent, the ^{13}C=O coupling to ^{15}N ($J_{CN} \sim 15$ Hz) result in splitting that translates to a loss in signal intensity and unnecessarily complicates the frequency spectrum. Refocusing of ^{13}C=O C_α coupling with frequency-selective inversion pulses can reverse the undesirable evolution of spin coherence at a specific time $t_1/2$ so that after further evolution to time t_1 it appears as if no carbonyl coupling is present.[1] This refocusing requires pulses that are highly frequency selective for both Zeeman and transverse magnetization, which turn out to be

(1) Brüschweiler, R.; Griesinger, C.; Sørensen, O. W.; Ernst, R. R. *J. Magn. Reson.* **1988**, *78*, 178.

0002-7863/92/1514-2108$03.00/0

important limitations in all but the most trivial experiments.[2] Furthermore, some experiments such as HNCA heteronuclear correlation[3] would require many selective decoupling pulses. Performing multiple rotations with selective pulses places severe requirements on the quality of these pulses as they should be compensated for offset, radio-frequency homogeneity and not attenuate or induce phase shifts in nearby resonances. For good selectivity and compensation, shaped pulses must be fairly long. The duration of the pulses places further restrictions on when and where they can be inserted into an experiment. In more general applications, selective refocusing can fail completely because of magnetization leakage to other coupling partners during the refocusing process.

An alternative to selective refocusing is selective decoupling, which prevents evolution by periodically scaling the coupling constant nearly to zero throughout the decoupling sequence. An ideal solution to the problem of carbonyl coupling would be to set a low-power decoupling sequence on the $^{13}C{=}O$ resonances, thereby removing the complications and imperfections of selective refocusing. If indirect detection methods are used, a fourth channel devoted to carbonyl decoupling could be left on continuously. This fourth carbonyl decoupling channel would eliminate amplitude and phase fluctuations associated with switching the decoupler on and off and would solve the problem of maintaining phase coherence during switches back and forth between the $^{13}C{=}O$ frequency and the region of interest (which is usually centered around the C_α resonances). In this paper we describe an amplitude-modulated waveform that allows for frequency-selective hetero- and homonuclear spin decoupling.

The motivation behind the development of decoupling sequences has been to obtain the largest bandwidth of decoupling for the smallest investment in power. To this end, the MLEV-16,[4] WALTZ-16,[5,6] and GARP-1[6,7] sequences have substantially improved the efficiency of broad-band decoupling. GARP-1 decouples efficiently over a bandwidth of $\pm 2.5\nu_2$, whereas WALTZ-16 is efficient over $\pm 1.25\nu_2$ and MLEV-16 is efficient over $\pm 1.0\nu_2$, where the strength of decoupling is measured in units of the peak Rabi frequency ν_2 (kHz) and is directly proportional to the intensity of the decoupling field B_2. Because these sequences were created solely for broad-band applications, their usefulness for selective decoupling is less obvious. Outside the decoupling bandwidth each sequence generates tremendous side bands, owing to the fact that each is a series of hard rectangular pulses with 180° phase shifts. The abrupt changes in amplitude and phase in these hard pulses produce high-frequency Fourier components that oscillate wildly far from resonance. In a sequence with close to 100 pulses and thousands of degrees of rotation, numerous large side bands are not suprising. Since broad-band sequences were never meant to be used selectively, the off-resonance oscillations represent nothing more than wasted energy.

Our strategy for selective decoupling uses the framework of the broadband decoupling sequences but replaces each 90° pulse element with a frequency-selective pulse shape. We start with the underlying $R\bar{R}\bar{R}R$ symmetry of the MLEV-16, WALTZ-16, and GARP-1 sequences. The building blocks of the WALTZ-16 sequence, 90°, 180°, 270°, and 360° flip angle pulses are straightforward to modify for selective decoupling. The composite inversion pulse WALTZ-4 is $R = \bar{3}4\bar{2}3\bar{1}2\bar{4}2\bar{3}$ where $1 = 90°$ and $\bar{1} = -90°$. In our selective decoupling sequence, each 90° pulse unit of WALTZ-4 is replaced with a shaped 90° pulse. We reasoned that since the sharp edges of each element can give rise to far-from-resonance oscillations, they can be eliminated without causing much deterioration to the decoupling within the sequence bandwidth. When combined in the $R\bar{R}\bar{R}R$ symmetry our selective shaped pulse becomes the shaped decoupling sequence in Figure 1.

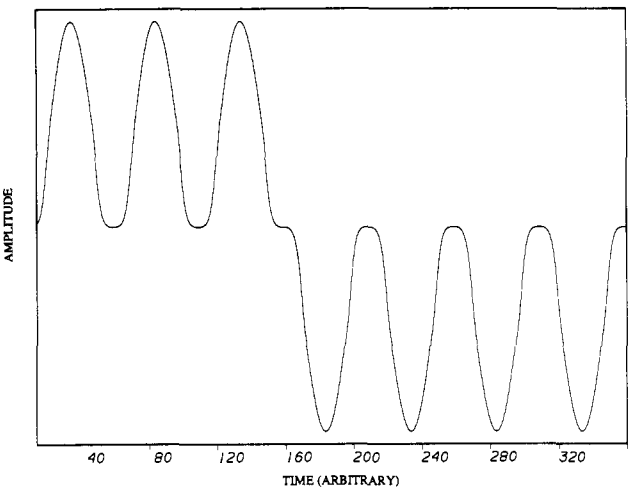

Figure 1. $\bar{3}4$ elements of the selective decoupling sequence where 4 is a 360° rotation provided by four selective 90° pulses (denoted $\overline{1111}$) and $\bar{3}$ is a 270° rotation provided by three 90° selective pulses ($\overline{111}$) where each $\bar{1}$ pulses are phase shifted 180° relative to 1. The 90° shaped pulses are designed to have minimum amplitude at the phase transitions and at the pulse edges of each 90° rotation so as to minimize spurious off-resonance excitation. We use, because of limitations of our waveform memory, a 4800-point waveform template for the sequence. All waveform synthesis was performed on a Varian Unity-600 spectrometer using their waveform memory board. Stand-alone waveform generation, though less versatile, may also be used especially when the decoupling sequence does not need to be coherently gated with other pulses.

Table I. 100-Point Approximation to the 90° Pulse Element of the Shaped Decoupling Sequence[a]

1	0.0	34	785.6	67	757.9
2	0.2	35	812.1	68	729.3
3	0.6	36	837.5	69	699.8
4	1.2	37	861.6	70	669.6
5	2.2	38	884.4	71	638.7
6	3.6	39	905.6	72	607.3
7	5.7	40	925.3	73	575.6
8	8.7	41	943.4	74	543.6
9	12.7	42	959.7	75	511.5
10	18.1	43	974.3	76	479.4
11	25.3	44	987.0	77	437.1
12	34.7	45	998.0	78	388.1
13	46.8	46	1006.9	79	336.0
14	62.2	47	1013.9	80	284.3
15	81.5	48	1019.0	81	235.0
16	105.5	49	1022.0	82	191.6
17	134.8	50	1023.0	83	153.3
18	169.8	51	1022.0	84	120.7
19	210.9	52	1019.0	85	93.7
20	257.7	53	1013.9	86	71.7
21	309.1	54	1006.9	87	54.1
22	363.5	55	998.0	88	40.2
23	417.7	56	987.0	89	29.3
24	468.4	57	974.3	90	21.0
25	511.5	58	959.7	91	14.8
26	543.6	59	943.4	92	10.1
27	575.6	60	925.3	93	6.7
28	607.3	61	905.6	94	4.2
29	638.7	62	884.4	95	2.5
30	669.6	63	861.6	96	1.4
31	699.8	64	837.5	97	0.7
32	729.3	65	812.1	98	0.3
33	757.9	66	785.6	99	0.1
				100	0.0

[a] The pulse maximum is 1023, and it is single phase. Of the entire sequence comprising 96 90° shaped pulses, only 180° phase shifts are used.

Many selective shaped 90° pulses perform miserably when used as inversion elements for selective decoupling sequences, whereas

(2) Emsley, L.; Bodenhausen, G. *Chem. Phys. Lett.* **1990**, *168*, 297. McCoy, M. A.; Mueller, L. *J. Magn. Reson.*, in press.
(3) Kay, L. E.; Ikura, M.; Tschudin, R.; Bax, A. *J. Magn. Reson.* **1990**, *89*, 496.
(4) Levitt, M.; Freeman, R. *J. Magn. Reson.* **1981**, *43*, 502. Levitt, M.; Freeman, R.; Frenkiel, T. *J. Magn. Reson.* **1982**, *47*, 328.
(5) Shaka, A. J.; Keeler, J.; Frenkiel, T.; Freeman, R. *J. Magn. Reson.* **1983**, *52*, 335.
(6) Shaka, A. J.; Keeler, J. *Prog. Nucl. Magn. Spectrosc.* **1987**, *19*, 47.
(7) Shaka, A. J.; Barker, P. B.; Freeman R. *J. Magn. Reson.* **1985**, *64*, 547.

the 90° unit of the shaped decoupling sequence (given in Table I) is, by itself, no more selective than a Gaussian pulse. Most selective pulse shapes are designed to perform single rotations: When used in composite sequences, their performance usually deteriorates markedly. The criteria used in the design of the shaped 90° unit emphasize the role of the pulse within a sequence and have little to do with the performance of individual elements of the sequence. Some of the features of the shaped decoupling sequence include a minimum amplitude in the transition regions to soften the phase shifts and a slightly tapered amplitude near the pulse maximum so that the overall pulse duration does not become excessive. The design of the shaped decoupling sequence uses a density matrix calculation to determine the on-resonance decoupling ability and the lack of off-resonance side bands for the entire decoupling sequence. The criteria used for determining which shaped pulse performs best and a rigorous comparison with the WALTZ-16 and GARP-1 decoupling sequences will be the subject of a subsequent paper.[8]

By modulating the amplitude of each 90° element of WALTZ-16, we obtain some desirable results. First, the elimination of most of the high-frequency Fourier components greatly attenuates the far-from-resonance oscillations, making frequency selectivity possible. Not surprisingly, we observe that for high-resolution decoupling (the scaling of a J coupling from 128 Hz to less than 1 Hz) the decoupling range offered by the shaped decoupling sequence $\pm 1.25\langle\nu_2\rangle$ is identical to the range offered by WALTZ-16 but inferior to the $\pm 2.5\langle\nu_2\rangle$ bandwidth of GARP-1 (where $\langle\nu_2\rangle$ is the average decoupler amplitude). For decoupling over the same spectral range, the power imparted to the sample using shaped decoupling is 45% more than the power delivered by WALTZ-16. For low-resolution decoupling (where the J coupling is scaled to $\sim$3 Hz), which is more applicable in protein NMR where the lines are typically broad, shaped decoupling extends its decoupling range to $\pm 1.75\langle\nu_2\rangle$. For the same low-resolution decoupling bandwidth, shaped decoupling uses about 70% of the power needed for WALTZ-16 decoupling but requires nearly 3 times more power than GARP-1 decoupling over the same decoupling interval. Using the lowest power, *broad-band* decoupling pulse is crucial; the pulse energy is dissipated by the sample by heating, which poses the most important limitation on high-power pulse decoupling. In selective decoupling, low B_2 fields are used and sample heating should not be an important limitation.

The selectivity of shaped decoupling for simple heteronuclear decoupling is compared with the low-power WALTZ-16 and GARP-1 sequences in Figure 2. A sample of [^{13}C]methyl propionate is used where the 128-Hz splitting of the methyl triplet in the proton spectrum is due to the heteronuclear J_{C-H} coupling. A hard rectangular pulse excites proton coherence, and during detection the labeled carbons are selectively decoupled by placing a low-power decoupling field at the methyl carbon resonance frequency. The decoupler offset is incremented in 15 steps, 600 Hz each, so that the effect of changing the decoupler offset on the quality of decoupling can, over a range of 9 kHz, be detected. The field intensities for the WALTZ-16, GARP-1, and shaped decoupling sequences, ν_2 = 425, 300, and 375 Hz, respectively, are roughly adjusted to reflect the calculated bandwidth of decoupling for each sequence. On resonance each sequence decouples moderately well. Since the decoupler field strength is low and the ^{13}C–H coupling is relatively large ($\nu_2/J \sim 3$, where $\nu_2/J \sim 10$ is recommended) and because synchronous sampling is impossible, decoupling of the quality found in the highest resolution work is unreasonable to expect. Nevertheless, good decoupling is observed over a relatively large bandwidth for all three sequences (although the $\pm 2\nu_2$ bandwidth achieved with GARP-1, which was used at a very low field intensity, is lower than expected). As we move away from resonance, the transition from uncoupled to coupled is rather gradual for WALTZ-16 and GARP-1 (strong modulation of the heteronuclear coupling is observed even at offsets of 9 kHz). Selective heteronuclear decoupling shows that the transition from decoupled to coupled occurs over $\sim$2 kHz. The off-resonance oscillations created by rectangular, phase-alternating decoupling sequences limit their use to broad-band applications. Using selective pulse elements but still retaining the supercycle symmetry, we are able to keep the benefits of WALTZ-16 decoupling without producing undesirable off-resonance effects.

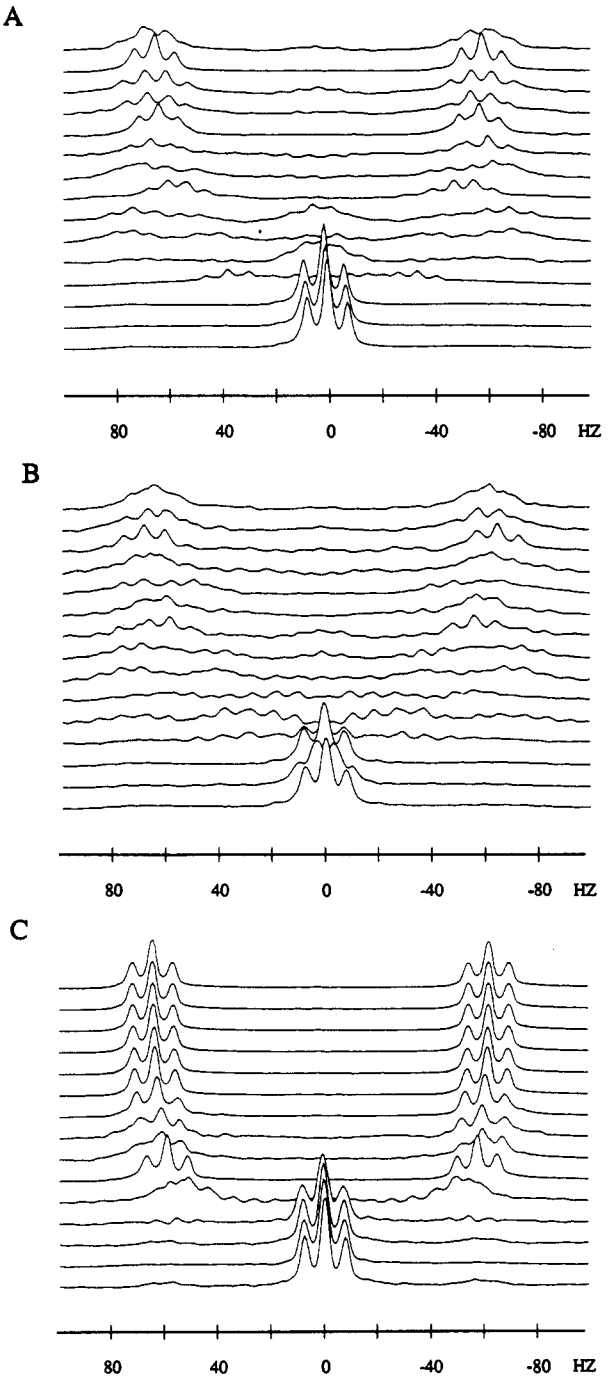

Figure 2. Decoupling dependence on offset for (A) WALTZ-16, (B) GARP-1, and (C) shaped selective decoupling of [^{13}C]methyl propionate. Selective decoupling with field strengths of (A) ν_2 = 425, (B) 300, and (C) 375 Hz was applied to the methyl carbon during proton detection after coherence was established with a hard ^{1}H rectangular excitation pulse. Weak WALTZ-16 and GARP-1 decoupling, as expected, generate large off-resonance oscillations which strongly modulate the heteronuclear coupling out to 9 kHz—30 times ν_2! Shaped decoupling offers roughly the same on resonance decoupling performance as WALTZ-16 or GARP-1, but the transition from decoupled to uncoupled is very sharp, occurring over just $\sim$2 kHz.

The best test of selectivity is not heteronuclear decoupling, which is rather easily accomplished, but homonuclear decoupling where nearby coherent magnetization should not be adversely affected

(8) McCoy, M. A.; Mueller, L. *J. Magn. Reson.*, in press.

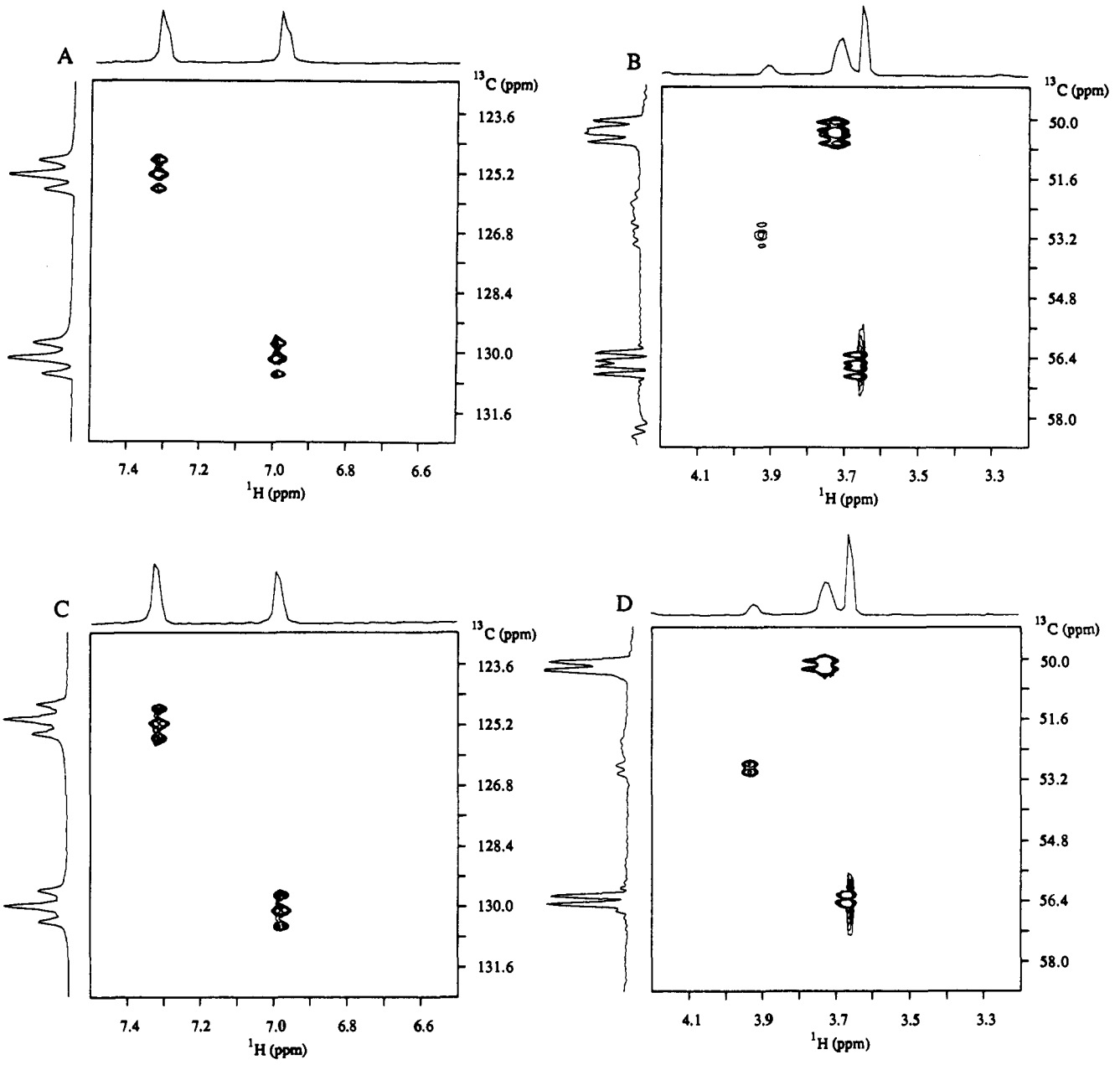

Figure 3. Expanded regions of the spectrum from an HMQC ^{1}H–^{13}C correlation experiment show (A) the aromatic region where tyrosine δ and ϵ correlation peaks split by ^{13}C–^{13}C couplings and (B) the aliphatic region where the dominant splitting is due to the 60-Hz ^{13}C=O C_α coupling. C and D are the aromatic and aliphatic regions, respectively, from an identical HMQC experiment only homonuclear carbonyl decoupling using shaped decoupling was used to remove the 60-Hz ^{13}C=O C_α coupling leaving (D) a 40-Hz doublet in the carbon dimension due to C_α–C_β coupling. A comparison of aromatic correlation peaks in the (A) coupled and (C) decoupled experiments shows that selective carbonyl decoupling does not modulate nearby aromatic carbon coherence.

by the decoupling pulse. A heteronuclear multiple quantum correlation experiment, or HMQC,[9] is performed to judge the quality and selectivity of homonuclear carbonyl decoupling. Peaks in the HMQC spectrum correlate carbon-decoupled proton chemical shifts in t_2 with carbon chemical shifts in t_1.

In Figure 3, the HMQC correlation spectra of a mixture of uniformly ^{13}C-labeled isoleucine, leucine, and tyrosine are compared with and without selective carbonyl decoupling. In the carbon spectrum, the carbonyl resonances are separated by 20 kHz from the C_α carbons but lie 7000 and 6300 Hz from the δ and ϵ aromatic carbon resonances, respectively, on the tryosine ring: The γ and ζ aromatic carbons are not proton coupled. The ^{1}H C_α correlation peaks of isoleucine, leucine, and tyrosine in Figure 3B show 60- and 40-Hz splitting in the carbon dimension due to ^{13}C=O and C_β coupling, respectively. The same HMQC experiment was repeated, only this time shaped decoupling, centered at the carbonyl resonance frequency and with a field intensity of ν_2 = 800 Hz, was on for the entire experiment. In Figure 3D the 60-Hz carbonyl coupling is removed from the C_α carbons, leaving the correlation peak, still split by the residual 40-Hz C_β coupling, a factor of two more intense. Figure 3A shows that only aromatic carbons coupled to protons are the δ and ϵ carbons, which are triplets due to two couplings of ~35 Hz each to neighboring carbons. A comparison between Figure 3A, without decoupling, and Figure 3C, with selective decoupling, shows that selective decoupling is sufficiently localized to not affect coherences formed by neighboring aromatic peaks.

In conclusion, we have demonstrated that, by amplitude modulation of single 90° pulse elements of the WALTZ-16 decoupling sequence, it is possible to achieve frequency-selective hetero- and homonuclear spin decoupling. Shaped decoupling

(9) Mueller, L. *J. Am. Chem. Soc.* **1979**, *101*, 4481. Bax, A.; Griffey, R. H.; Hawkins, B. L. *J. Magn. Reson.* **1983**, *55*, 301.

offers efficient on-resonance decoupling over a large bandwidth and is well compensated for both radio-frequency inhomogeneity and flip angle errors because it is constructed with the same global symmetry as are the WALTZ, MLEV, and GARP supercycles. Although the quality of decoupling near resonance is not affected by amplitude modulation, spurious oscillations created far from resonance by traditional decoupling sequences are dramatically attenuated. Shaped decoupling can be operated at very low field strengths so as not to induce perturbations in noncoupled coherences. Shaped decoupling should virtually eliminate complications from carbonyl coupling in multidimensional spectra of labeled proteins and lend itself to other applications where selective decoupling is desirable.

Acknowledgment. We thank Tom McVarish for reviewing this manuscript.

Determination of Structures of Solvated Lithium Dialkylamides by Semiempirical (MNDO) Methods. Comparison of Theory and Experiment

Floyd E. Romesberg and David B. Collum*

Contribution from the Department of Chemistry, Baker Laboratory, Cornell University, Ithaca, New York 14853-1301. *Received August 12, 1991*

Abstract: MNDO computational studies of lithium dimethylamide (Me_2NLi), lithium diisopropylamide (LDA), and lithium 2,2,6,6-tetramethylpiperidide (LiTMP) solvated by H_2O, Me_2O, THF, phosphoramide ($(NH_2)_3P{=}O$), and hexamethylphosphoramide (HMPA) are described. The relative stabilities of monomers, dimers, trimers, open dimers, and anionic triple ions reveal the steric and electronic factors that influence aggregation state. The calculations support previous suggestions that coordinated solvents destabilize cyclic trimers relative to cyclic dimers. The cyclic dimers appear to be most stable in the disolvated form (one solvent per lithium). The increased steric demands of *N*-alkyl moieties cause decreased stabilities of cyclic dimers relative to the monomers, open dimers, and triple ions. The optimized structures of open dimers and triple ions reveal relative rotations of the amide fragments and increased internal N-Li-N bond angles consistent with considerable relief of steric interactions. Direct comparisons between calculated structures of various HMPA and THF solvates of LDA and LiTMP with previously described solution structure studies reveal excellent correlations of theory and experiment.

Introduction

For several years we have been investigating the solution structures of lithium dialkylamides, lithiated hydrazones, and lithioimines with the long-term goal of understanding the determinants of organolithium selectivity and reactivity.[1-13] Although a combination of NMR spectroscopic and kinetic methods can deconvolute the structures[1-7] and consequences of the various aggregation states,[6,8-12] there are fundamental issues associated with solvation that remain acutely elusive. There are only a handful of instances in the vast organolithium literature in which solvation states have been determined in solution,[4,5,7,14-16] and most of these are based on relatively indirect methods.

Scheme I

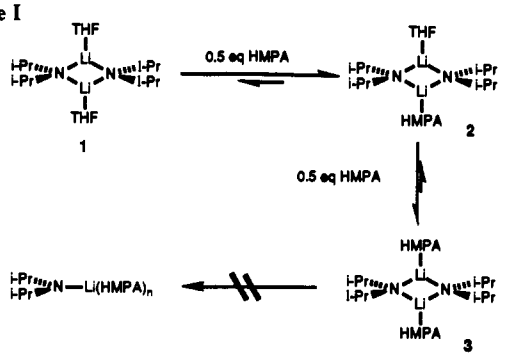

(1) For leading references, see: Kim, Y.-J.; Bernstein, M. P.; Galiano-Roth, A. S.; Romesberg, F. E.; Williard, P. G.; Fuller, D. J.; Harrison, A. T.; Collum, D. B. *J. Am. Chem. Soc.* **1991**, *113*, 5053.
(2) Hall, P. L.; Gilchrist, J. H.; Harrison, A. T.; Fuller, D. J.; Collum, D. B. *J. Am. Chem. Soc.* **1991**, *113*, 9175.
(3) Kim, Y.-J.; Bernstein, M. P.; Galiano-Roth, A. S.; Romesberg, F. E.; Williard, P. G.; Fuller, D. J.; Harrison, A. T.; Collum, D. B. *J. Org. Chem.* **1991**, *56*, 4435.
(4) Kallman, N.; Collum, D. B. *J. Am. Chem. Soc.* **1987**, *109*, 7466.
(5) Depue, J. S.; Collum, D. B. *J. Am. Chem. Soc.* **1988**, *110*, 5518.
(6) Galiano-Roth, A. S.; Collum, D. B. *J. Am. Chem. Soc.* **1988**, 3546.
(7) Wanat, R. A.; Collum, D. B.; Van Duyne, G.; Clardy, J.; DePue, R. T. *J. Am. Chem. Soc.* **1986**, *108*, 3416. Jackman, L. M.; Scarmoutzos, L. M.; DeBrosse, C. W. *J. Am. Chem. Soc.* **1987**, *109*, 5355.
(8) Romesberg, F. E.; Gilchrist, J. H.; Harrison, A. T.; Fuller, D. J.; Collum, D. B. *J. Am. Chem. Soc.* **1991**, *113*, 5751.
(9) Galiano-Roth, A. S.; Collum, D. B. *J. Am. Chem. Soc.* **1989**, *111*, 6772.
(10) Depue, J. S.; Collum, D. B. *J. Am. Chem. Soc.* **1988**, *110*, 5518; 5524.
(11) Bernstein, M. P.; Romesberg, F. E.; Fuller, D. J.; Harrison, A. T.; Collum, D. B.; Liu, Q.-Y.; Williard, P. G. *J. Am. Chem. Soc.*, in press.
(12) Hall, P. L.; Gilchrist, J. H.; Collum, D. B. *J. Am. Chem. Soc.* **1991**, *113*, 9171.
(13) Gregory, K.; Schleyer, P. v. R.; Snaith, R. *Adv. Organomet. Chem.*, in press.
(14) Brown, T. L.; Gerteis, R. L.; Rafus, D. A.; Ladd, J. A. *J. Am. Chem. Soc.* **1964**, *86*, 2135. Lewis, H. L.; Brown, T. L. *J. Am. Chem. Soc.* **1970**, *92*, 4664. Quirk, R. P.; Kester, D. E. *J. Organomet. Chem.* **1977**, *127*, 111. Bartlett, P. D.; Goebel, C. V.; Weber, W. P. *J. Am. Chem. Soc.* **1969**, *91*, 7425. Cheema, Z. K.; Gibson, G. W.; Eastham, J. F. *J. Am. Chem. Soc.* **1963**, *85*, 3517. Eastham, J. F.; Gibson, G. W. *J. Am. Chem. Soc.* **1963**, *85*, 2171. Waack, R. Doran, M. A.; Stevenson, P. E. *J. Am. Chem. Soc.* **1966**, *88*, 2109. Bauer, W.; Klusener, P. A. A.; Harder, S.; Kanters, J. A.; Duisenberg, A. J. M.; Brandsma, L.; Schleyer, P. v. R. *Organometallics* **1988**, *7*, 552. Harder, S.; Boersma, J.; Brandsma, L.; Kanters, J. A.; Bauer, W.; Pi, R.; Schleyer, P. v. R.; Schölhorn, H.; Thewalt, U. *Organometallics* **1989**, *8*, 1688. Bauer, W.; Schleyer, P. v. R. *J. Am. Chem. Soc.* **1989**, *111*, 7191. Fraenkel, G.; Chow, A.; Winchester, W. R. *J. Am. Chem. Soc.* **1990**, *112*, 1382. Quirk, R. P.; McFay, D. *J. Polym. Sci., Polym. Chem. Ed.* **1981**, *19*, 1445. Wehman, E.; Jastrzebski, J. T. B. H.; Ernsting, J.-M.; Grove, J. M.; van Koten, G. *J. Organomet. Chem.* **1988**, *353*, 145.
(15) Reich, H. J.; Gree, D. P. *J. Am. Chem. Soc.* **1989**, *111*, 8729. Reich, H. J.; Green, D. P.; Phillips, N. H. *J. Am. Chem. Soc.* **1989**, *111*, 3444. Reich, H. J.; Borst, J. P. *J. Am. Chem. Soc.* **1991**, *113*, 1835.

0002-7863/92/1514-2112$03.00/0